

Proposal of a New Binding Orientation for Non-Peptide AT1 Antagonists: Homology Modeling, Docking and Three-Dimensional Quantitative Structure–Activity Relationship Analysis

Tiziano Tuccinardi,[†] Vincenzo Calderone,[‡] Simona Rapposelli,[†] and Adriano Martinelli^{*,†}

Dipartimento di Scienze Farmaceutiche, Università di Pisa, via Bonanno 6, 56126 Pisa, Italy, and Dipartimento di Psichiatria, Neurobiologia, Farmacologia e Biotecnologie, Università di Pisa, via Bonanno 6, 56126 Pisa, Italy

Received March 23, 2006

A three-dimensional model of the AT1 receptor was constructed by means of a homology modeling procedure, using the X-ray structure of bovine rhodopsin as the initial template and taking into account the available site-directed mutagenesis data. The docking of losartan and its active metabolite EXP3174, followed by 1 ns of molecular dynamics (MD) simulation inserted into the phospholipid bilayer, suggested a different binding orientation for these antagonists from those previously proposed. Furthermore, the docking of several non-peptide antagonists was used as an alignment tool for the development of a three-dimensional quantitative structure–activity relationship (3D-QSAR) model, and the good results confirmed our binding hypothesis and the reliability of the model.

Introduction

The renin–angiotensin–aldosterone system (RAAS) is a proteolytic cascade that plays an important role in electrolyte homeostasis and in the regulation of blood pressure, but it is also involved in the pathogenesis of hypertension and renal diseases.

The RAAS begins with the release of the aspartic protease renin from the juxtaglomerular cells of the kidney. This enzyme is responsible for the conversion of angiotensinogen to the inactive decapeptide angiotensin I. In turn, angiotensin I is cleaved by the angiotensin-converting enzyme (ACE) to produce the octapeptide angiotensin II (AngII), which is the main effector hormone of the RAAS.

AngII is the major regulator of blood pressure, electrolyte balance, and endocrine functions related to cardiovascular diseases such as hypertension. Moreover, it has been shown that AngII plays a role in various pathological situations involving tissue remodeling, such as cardiac hypertrophy. Recent findings^{1,2} indicate the involvement of this peptide also in cancer.

AngII affects most of the biological functions by activating selective membrane-bound receptors. Two distinct subtypes of AngII receptors [type 1 (AT1) and type 2 (AT2)] have been identified, and both belong to the G protein-coupled receptor superfamily (GPCRs).

AT1 and AT2 are seven-transmembrane-spanning receptors, comprising an extracellular glycosylated region connected to the seven transmembrane α -helices, which are linked by three intracellular and three extracellular loops. The carboxy-terminal domain of the protein is cytoplasmic and is a regulatory site. AT1 is a 359-amino acid protein, while AT2 is made up of 363 amino acid and is 30% homologous with AT1. Both receptors are N-linked glycosylated post-translationally.

AT1 receptors are expressed in various parts of the body and mediate all of the known effects associated with AngII, such as vasoconstriction, aldosterone release, and other functions that tend to elevate blood pressure and cause hypertrophy and

hyperplasia of target cells. By contrast, AT2 receptors are most highly expressed in fetal tissue, in which they are responsible for mediating organ remodeling, whereas they are sparsely represented in the adult and appear only at the site of inflammation, tissue damage, or other forms of cellular stress such as ischemia. The AT2 receptor seems to be responsible for both the inhibition of cell growth and the promotion of apoptosis.³ Although the role of the AT2 receptor is less fully understood, it is usually believed to have opposing effects to the AT1 receptor.

Given the important role played by the RAAS in hypertension, this system is the main target of any effective therapy. The first choice class of drugs to influence the RAAS targeting is that of ACE inhibitors.

These drugs block the formation of AngII and also prevent the conversion of bradykinin to inactive peptides. Although bradykinin may contribute to the beneficial effects of ACE inhibitors through its vasorelaxing effect, its accumulation determines some disadvantages such as the development of coughing and angioedema, which are side effects often associated with ACE-inhibitor therapy. Moreover, ACE inhibitors do not completely suppress AngII, because its formation is ensured also by ACE-independent pathways. For these reasons, it was particularly important when AngII subtype 1 receptor antagonists (AT1 antagonists or sartans) were developed as a new class of antihypertensives used in the treatment of hypertension,⁴ heart failure,⁵ and renal diseases.⁶ Although precise mechanisms have not yet been elucidated to explain all of the beneficial effects, sartans are unique in their ability to provide such benefits with a limited side-effect profile.⁷

The first non-peptide AT1 antagonist, which represents the prototype of the sartans, was losartan. The major active metabolite of losartan, EXP3174, generated by the oxidation of the 5-hydroxymethyl group on the imidazole ring, is 10–40 times more potent than losartan itself and thus accounts for the majority of its pharmacological activity.

At present, many selective, potent, and orally available sartans have been developed and are used to treat both hypertension and damage associated with diseases such as atherosclerosis and diabetes.

Although all sartans bind with a high affinity to the AT1 receptor and share a common mechanism of action, there are

* E-mail: marti@farm.unipi.it. Fax: ++39 050 2219605. Tel: ++39 050 2219556.

[†] Dipartimento di Scienze Farmaceutiche.

[‡] Dipartimento di Psichiatria, Neurobiologia, Farmacologia e Biotecnologie.

differences in the modes of interaction with the receptor.^{8,9} Sartans such as losartan, eprosartan, and tasosartan bind to the receptor with different degrees of surmountability. Valsartan, irbesartan, candesartan, and the active metabolite of losartan (EXP3174) behave like insurmountable antagonists.

A possible explanation for this different response is that the surmountable antagonists interfere with receptor activation by occupying an intramembrane site that overlaps with the space occupied by the agonist, while insurmountable antagonists induce conformational changes that prevent agonist binding. Another theory hypothesizes that surmountable antagonists dissociate rapidly from the receptor, whereas insurmountable antagonists bind tightly and dissociate so slowly as to cause a prolonged functional loss of the occluded receptors.¹⁰

A knowledge of the 3D structure of the AT1 receptor could be of great help in the task of understanding antagonists interaction and in the rational design of specific ligands; however, because GPCRs are membrane-bound proteins, high-resolution structural characterization is still an extremely difficult task.

Several studies have been performed to investigate the binding site of the AT1 receptor, and the disposition of its residues; on the basis of all this information, a homology model of the human AT1 receptor was constructed in the present study, and surmountable and insurmountable antagonists were docked.

Furthermore, to obtain a quantitative model capable of measuring the reliability of the receptor constructed and also to provide a predictive system that could be exploited for the design of new AT1 antagonists, a three-dimensional quantitative structure–activity relationship (3D-QSAR) model was calculated, based on the alignment obtained by docking several ligands into the AT1 receptor.

Results and Discussion

Homology Modeling. The AT1 receptor model was generated using the recent bovine rhodopsin crystal structure determined at 2.2 Å (1U19¹¹) as the template. The sequence alignment was studied on several AngII receptors. As shown in Figure 1, the alignment was guided by the highly conserved amino acid residues, including the asparagine residues N1.50, the LA-AD (L2.46, A2.47, A2.49, and D2.50), and D/ERY- -V (D/E3.49, R3.50, Y3.51, and V3.54) motif, the highly conserved tryptophane W4.50, the two prolines P4.59 and P6.50, and the NPXXY motif in TM7 (N7.49, P7.50, and Y7.53).¹²

On the basis of this alignment, the AT1 receptor model was built and was then subjected to a simulated annealing protocol by means of the Modeller program.¹³ The backbone conformation of the best scored structure was evaluated by using the PROCHECK software¹⁴ (see Experimental Section for details), and an analysis of the ψ/ϕ Ramachandran plot indicated that only two amino acids of the loop fragments (H24 and S186) had a disallowed geometry.

The results obtained suggested that the molecular model of the AT1 receptor created could be used for further studies.

Docking of Losartan. Site-directed mutagenesis suggested an important role for many residues; in particular, the affinity of losartan seemed to be mainly influenced by the presence of K3.24(102), K5.42(199),¹⁵ V3.32(108), A4.60(163),¹⁶ and N7.46(295)¹⁷ (even if this last residue might be responsible for the conformational changes that occur in AT1 receptor activation^{18,19}).

The analysis of the disposition of these residues in the AT1 receptor model highlighted that, with the exception of K3.24-(102) which was far away and directed toward the extracellular

side of the receptor, all the others residues were comprised in a limited region compatible for the interaction with losartan. Furthermore aligning the AT1 receptor model with the bovine rhodopsin crystal structure came out that the residues listed above (principally V3.32(108), K5.42(199), and N7.46(295)) delimited a region that corresponded to the binding site of retinal.

Bearing all these things in mind, the non-peptide antagonist losartan was docked into the AT1 receptor model, using the AUTODOCK program²⁰ and building a “docking box” that included the main mutagenesis data (see Experimental Section for details).

The best docked structure of losartan highlighted an interaction of the hydroxymethyl substituent with K5.42(199), while V3.32(108) interacted with the biphenyl system, and A4.60-(163) with the *n*-butyl substituent; N7.46(295) seemed not to interact with the ligand.

As regards the role of the tetrazole ring in AT1 receptor binding, all the recent models suggest an ionic interaction with K5.42(199),^{17,21} even if there is no experimental evidence confirming it; it does not seem possible, therefore, to exclude other binding dispositions “a priori”.

In our docking analysis, the tetrazole ring did not appear to interact with any residue indicated as important by mutagenesis studies, but instead it appears to be capable of accepting a H bond from Y184, and this orientation was used as the starting point for further refinement and evaluation.

Thus the losartan–AT1 receptor complex was refined by means of 1 ns of molecular dynamics (MD) simulation.

A vacuum MD simulation can lead to severe distortions, especially of the loop structures, and the primary source of these distortions appears to be the formation of artificial H bonds.²² Furthermore, a vacuum MD simulation requires the use of a set of restraints to replace the natural stabilizing effects of the membrane bilayer on the TM domains, reducing the free movement of the helices. To avoid these problems, we carried out the simulation in a fully hydrated phospholipid bilayer environment made up of dipalmitoylphosphatidylcholine (DPPC) molecules solvated by TIP3 water molecules as described in the Experimental Section.

The system contained 192 DPPC molecules, 7410 water molecules, 16 chlorine atoms, the AT1 receptor, and losartan, for a total of 52 940 atoms.

The stability of the model was evaluated by calculating the total energy of the system; as shown in Figure 2A, after 400 ps of MD, the system reached an equilibrium, since the total energy for the last 600 ps remained approximately constant. Analyzing the root-mean-square deviation (RMSD) of all the α carbons of the TM helices from the starting AT1 model structure, we observed that after an initial increase, in the last 400 ps the RMSD remained between the values of 1.5 and 1.8 Å (see Figure 2B), suggesting that our MD procedure was correct.

Figure 3 shows the AT1–losartan complex embedded into the DPPC bilayer; the binding site was limited by TM3, -4, -5, -6, and -7 and the second extracellular loop (EL2). As regards losartan, it showed the tetrazole ring and the hydroxymethyl substituent turned in the direction of the extracellular side of the receptor.

Biophysical studies showed that losartan interacts with the interface of phospholipid membranes;^{23,24} on the basis of these studies, Zoumpoulakis et al.²¹ hypothesized that losartan binds to the receptor after a first step that involves incorporation and interaction with membrane bilayers. As for the location of losartan in the phospholipid core, it was found to be situated

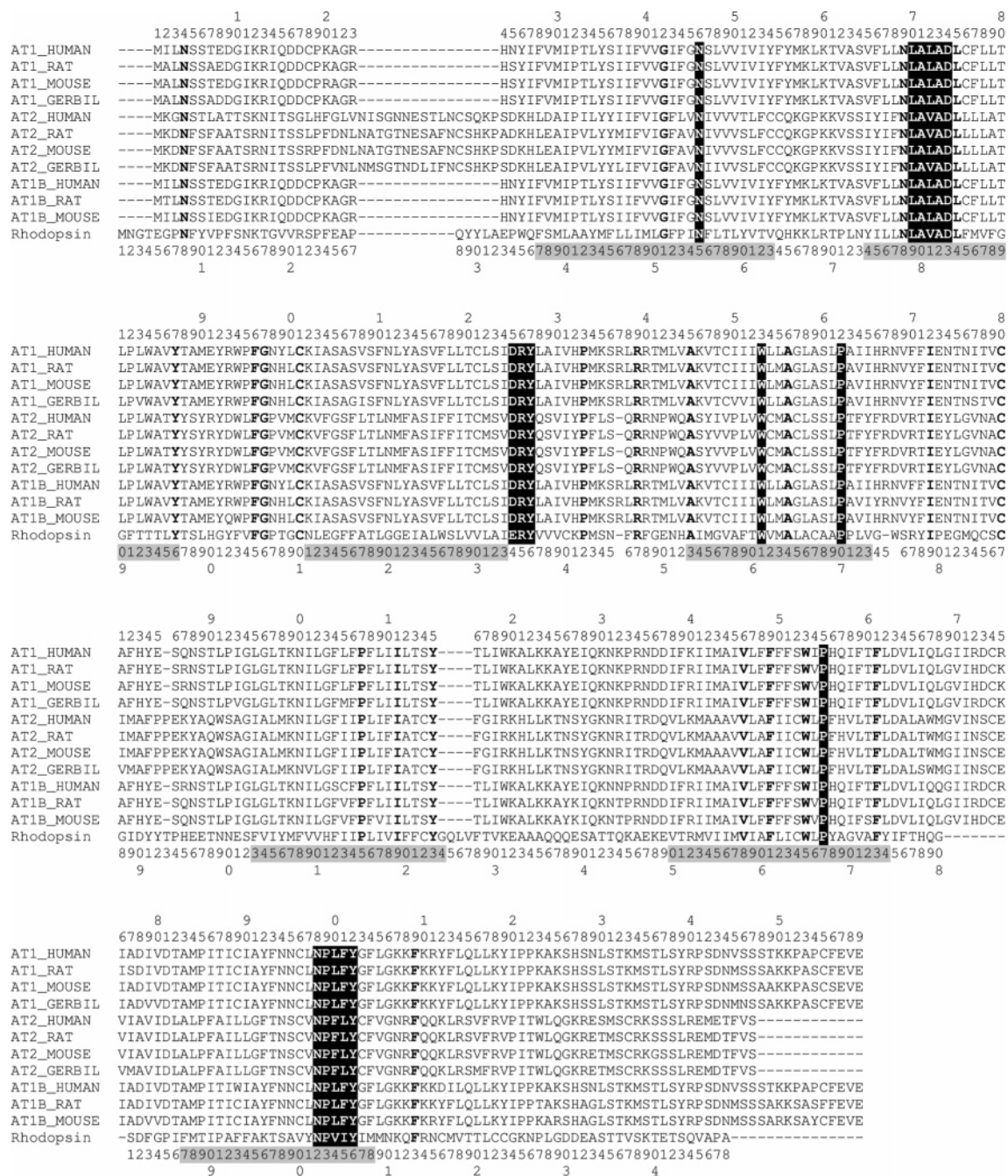


Figure 1. Alignment of the AngII receptors and bovine rhodopsin amino acid sequences. The highly conserved patterns of the LA-AD (L2.46, A2.47, A2.49, and D2.50), D/ERY motif (D/E3.49, R3.50, and Y3.51), the highly conserved tryptophane W4.50, the two prolines P4.59 and P6.50, and the NPXXY motif in TM7 (N7.49, P7.50, and Y7.53) are marked with black. The other identical residues are in bold. In the first and in the last line of the alignment scheme are reported the numerations of the human AT1 and bovine rhodopsin, respectively, while the TM domains of bovine rhodopsin are reported in gray.

near the interface and exhibited a H bond between the hydroxymethyl group and the phospholipid phosphate group, while the tetrazole substituent interacted with four $N^+(CH_3)_3$ headgroups of the phospholipid. The binding conformation of losartan obtained in our MD simulation and its disposition inside the receptor were compatible with this possible mechanism of interaction. The position of the antagonist was in the upper part of the receptor, in the region between the TM3–7 helices; furthermore, the losartan conformation inside the receptor was similar to the one that, according to the Zoumpoulakis's hypothesis, is capable of interacting in the membrane.

Figure 4 shows the binding site of losartan in the AT1 receptor. The biphenyl ring of the antagonist was positioned between TM3, TM6, and TM7 in a lipophilic cavity principally

delimited by V3.32(108), V179, W6.48(253), H6.51(256), I7.39-(288), and Y7.43(292). The anionic tetrazole group was directed toward the extracellular side of the receptor and interacted with T175 and Y184, which are two residues of EL2, forming a third H bond with H6.51(256). As regards the 2'-butyl substituent, it was directed toward TM4 and interacted in a secondary lipophilic pocket created by S3.33(109), L3.36(112), Y3.37-(113), A4.60(163), F171, and F182 of EL2, while the hydroxymethyl group formed a H bond with K5.42(199).

Over the last three years, studies on the AT1 receptor using the substituted-cysteine accessibility method (SCAM)^{25,26} and the methionine proximity assay²⁷ have investigated the disposition of the residues belonging to TM3, TM6, TM7, and part of EL3. More in detail, these studies suggest that A3.28(104),

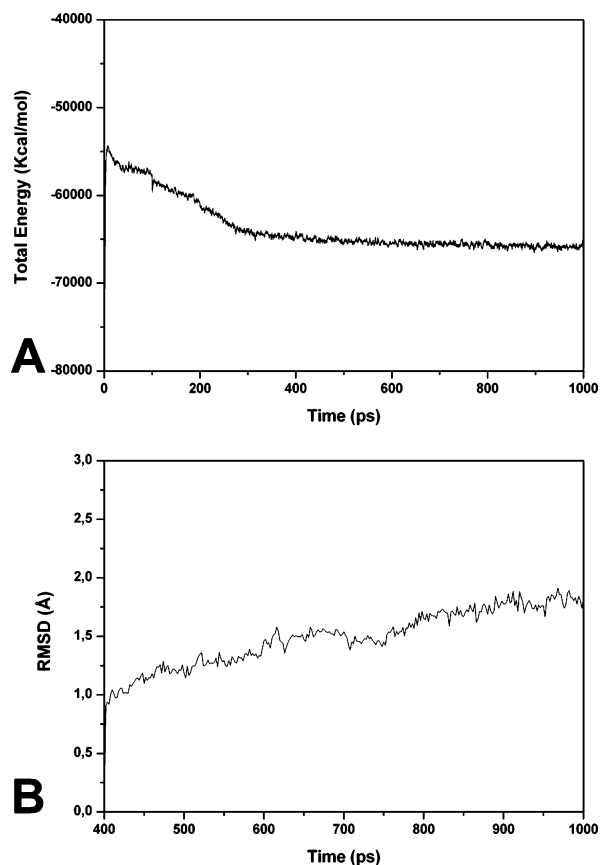


Figure 2. Analysis of the MD simulation of losartan complexed with AT1. In the first plot (A), the total energy of the system vs the time is reported; in the second plot (B), the RMSD between all the α carbons of the TM helices is reported.

N3.35(111), L3.36(112), Y3.37(113), F6.44(249), W6.48(253), H6.51(256), T6.55(260), A277, V280, T7.33(282), A7.34(283), I7.37(286), A7.42(291), F7.44(293), N7.45(294), N7.46(295), C7.47(296), L7.48(297), and F7.52(301) should be oriented within the water-accessible crevice of the AT1 receptor, and in our receptor model, only A7.34(283), I7.37(286), and F7.44(293) among all these residues were not oriented within the water-accessible crevice. However, as regards F7.44(293), the authors suggested that the terminal part of the TM7 structure is somewhat destabilized, thus allowing outward-pointing residues to turn intermittently inward.²⁷

As regards the interaction of losartan in the AT1 receptor, site-directed mutagenesis suggested the importance of V3.32(108).¹⁶ In 1995, Noda et al.¹⁵ revealed that mutation of K5.42(199) with alanine, glutamate, and arginine determined a more-than-10-fold decrease in binding affinity, while the mutation of lysine with glutamine determined only a 2-fold decrease of losartan affinity. With regards to H6.51(256), Takezako et al.¹⁷ pointed out that the mutation with alanine determined an important affinity decrease only when accompanied by the K5.42(199)A mutation, suggesting a complementary role for H6.51(256), whereas for the mutation H6.51(256)A, Noda et al.¹⁵ reported a 2-fold decreases in the affinity of losartan. Thus all these studies were in agreement with our AT1–losartan model.

Other mutagenesis studies suggested a fundamental role for the residues D2.50(74), N3.35(111), S3.39(115), N7.45(294), and N7.46(295) in the process of activation of the receptor.^{18,19,28–31} In our model, these residues were not directly involved in the interaction with losartan, but as shown in Figure 5, they interacted with each other, creating a H bond network

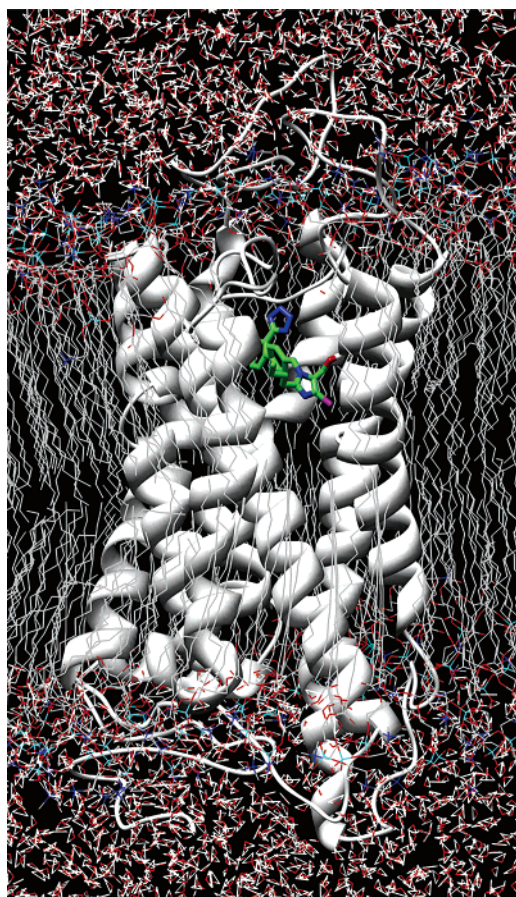


Figure 3. Losartan–AT1 receptor complex inserted in the DPPC bilayer model.

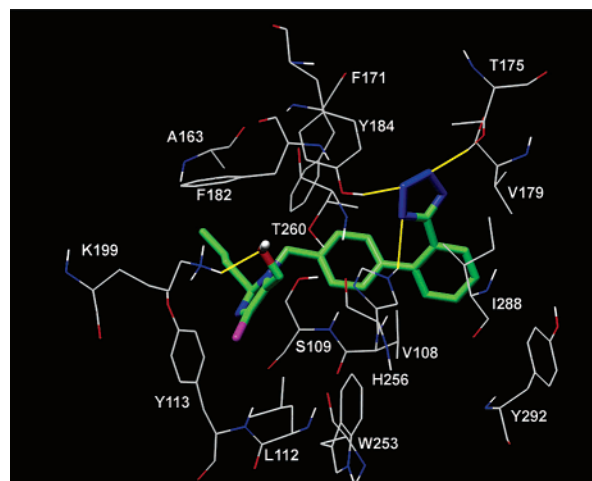


Figure 4. Losartan docked in the AT1 binding site. Interatomic distances between H-bonded atoms are indicated in yellow.

system able to connect TM2, TM3, and TM7, probably controlling the inactive–active state of the receptor.

Thus these observations were in agreement with the hypothesis of a “structural role” for N7.46(295), instead of a direct interaction with losartan.^{18,19}

Docking of Insurmountable Antagonists. To investigate the binding characteristics deriving from the interaction of an insurmountable antagonist, starting from the AT1 receptor model obtained through the simulated annealing protocol, we used the Autodock program²⁰ to dock the active metabolite of losartan (EXP3174) (see Experimental Section for details).

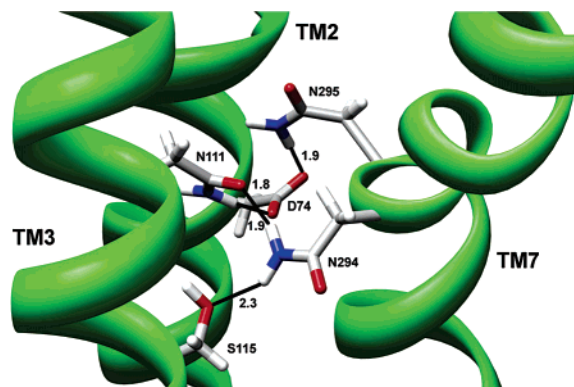


Figure 5. H bond network system among TM2, TM3, and TM7 of the AT1 receptor model.

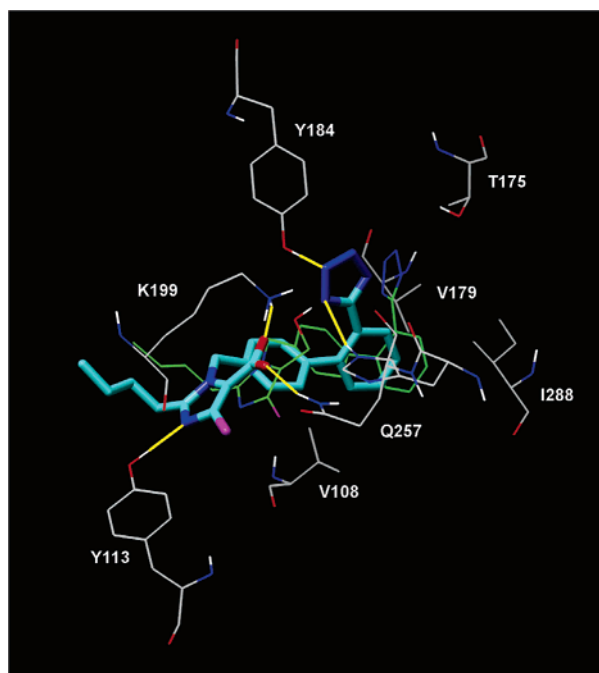


Figure 6. Superimposition between EXP3174 (sky blue) and losartan (green) docked in the AT1 binding site.

Subsequently, the complex of best docked structure with the AT1 receptor was subjected to 1 ns of MD, using the same protocol applied for losartan.

The results obtained from the MD simulation showed that the binding disposition of the ligand was similar to that of losartan with the biphenyl ring located in the lipophilic pocket delimited by V3.32(108), V179, W6.48(253), H6.51(256), I7.39(288), and Y7.43(292) and the 2'-butyl substituent interacting in the secondary lipophilic pocket created by S3.33(109), L3.36(112), Y3.37(113), A4.60(163), F171, and F182. However as shown in Figure 6, with respect to losartan, EXP3174 was shifted about 2.7 Å toward TM5. This disposition determined the loss of the H bond of tetrazole with T175, which proved to be too distant (5.3 Å from the tetrazole ring), while the interaction with Y184 and H6.51(256) was maintained.

As regards the imidazole ring, it exhibited a new H bond with Y3.37(113), while the carboxylate group interacted with K5.42(199) and also formed a second H bond with Q6.52(257).

It transpired from this analysis that even though EXP3174 did not interact with T175 like losartan, it displayed two additional interactions with Y3.37(113) and Q6.52(257). Furthermore, the carboxylate group formed an ionic interaction with

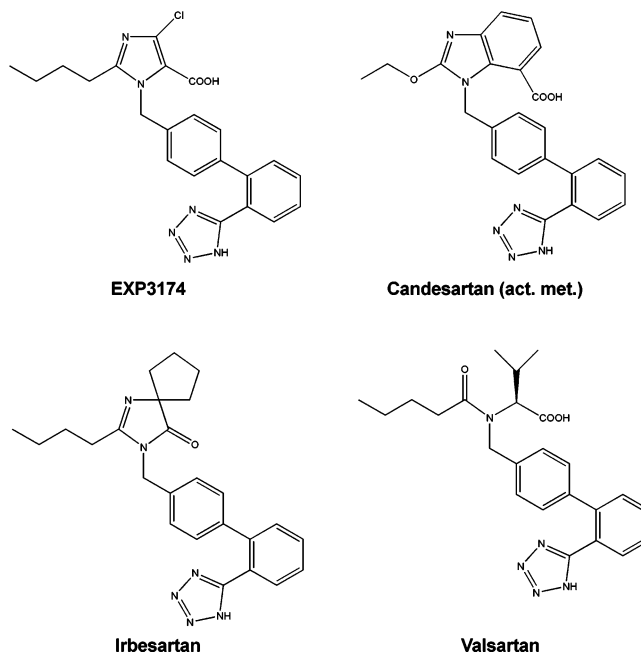


Figure 7. Insurmountable antagonists used in the docking study (for candesarant, its active metabolite was reported).

K5.42(199), which should be stronger than the H bond interaction of the hydroxymethyl group of losartan.

Overall, it appeared that the EXP3174–AT1 binding interaction was stronger than the losartan–AT1 interaction; these observations were in agreement with the hypothesis that unlike surmountable antagonists, insurmountable antagonists could bind tightly and dissociate slowly, causing the functional loss of the occluded receptors.¹⁰

Furthermore, the interactions of the carboxylate group with K5.42(199) and Q6.52(257) were in agreement with site-directed mutagenesis data, which suggested a fundamental role for these two residues in insurmountable antagonist binding.^{17,32}

To verify whether interaction with K5.42(199) and Q6.52(257) was only a peculiarity of EXP3174 or, as suggested by mutagenesis data, it was displayed also by other insurmountable antagonists, we used the receptor obtained through the simulation with EXP3174 to dock the other three insurmountable antagonists, candesarant, irbesartan, and valsartan (see Figure 7) by means of an automated docking procedure (see Experimental Section for details).

As shown by Figure 8, all the ligands exhibited a binding disposition very similar to that of EXP3174. Furthermore, K5.42(199) and Q6.52(257) were involved in the binding of all three ligands, interacting with the carboxylate group of candesarant (B) and valsartan (D) and the carbonylic oxygen of irbesartan (C).

3D-QSAR. In the past years, several 3D-QSAR and pharmacophore studies on the AT1 receptor antagonists have been performed and reported in the literature.^{33–40} All these studies were characterized by a ligand-based alignment for the development of predictive models.

In this paper, on the basis of the information derived from an AT1 receptor homology model, the possibility of developing a 3D-QSAR model was investigated.

For these reasons, and also for verifying the reliability of this modeled AT1 receptor, 62 non-peptide antagonists^{41–43} (see Table 1) were docked into the AT1 receptor, and for each ligand, the best docked conformation was used for the development of a 3D-QSAR model (see Experimental Section).

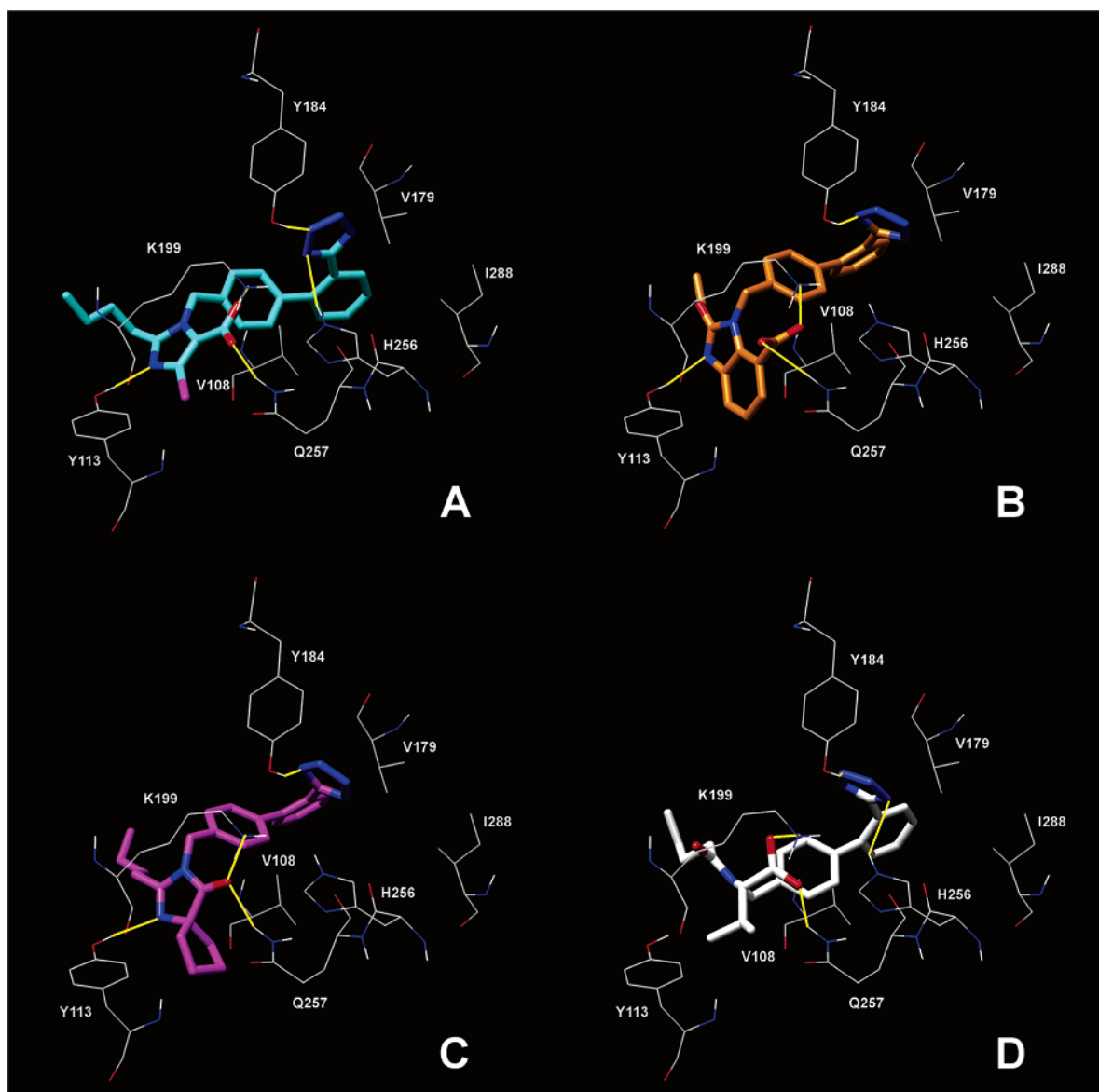


Figure 8. Docking of EXP3174 (A), candesartan (B), irbesartan (C), and valsartan (D) in the AT1 binding site. Interatomic distances between H-bonded atoms are indicated in yellow.

3D-QSAR analysis was carried out using different probes (see Experimental Section for details). To measure the reliability of the different probes, the 3D-QSAR models were characterized by their correlation coefficient (r^2), predictive correlation coefficient (q^2), and cross-validated standard deviation of errors of prediction ($SDEP_{CV}$). Table 2 summarizes the three best models obtained, respectively, with the C3, the OH probe, and a combination of them. These data indicated that the OH probe seemed to be the best one.

Furthermore, an external test set of 10 antagonists (marked with an asterisk in Table 1) were used to test the predictive ability of the models, and this analysis confirmed that the OH probe was the best selection ($SDEP_{test-set} = 0.54$, see Table 2 and Figure 9).

To further evaluate the predictive ability of the models, a new data set of 25 AT1 antagonists were retrieved from literature⁴⁴ and used as a second test set.

Also for this analysis, the OH probe was confirmed to be the best selection, as it showed the lower $SDEP_{test-set}$ value (see Table 3 and Figure 9).

One important feature of 3D-QSAR analysis is the graphic representation of the model, usually aimed at making its

interpretation easier. In the GOLPE program,⁴⁵ there are several options for displaying the final model. Among these, the PLS pseudo-coefficient and the activity contribution plots are very useful. The PLS coefficient plot makes it possible to visualize favorable and unfavorable interactions between the probes and the molecules under study, while the activity contribution plot is different for every molecule within the training set and makes it possible to display spatial regions that are individually important for the selected molecule.

Figure 10A,B illustrates the PLS coefficients plots of model 2. Figure 10A shows negative PLS coefficients; in particular, there are eight principal regions (A–H) with negative values, in which a favorable interaction between a substituent and the probe determines an increase in activity, whereas an unfavorable interaction between a substituent and the probe determines a decrease in activity. In contrast, the positive PLS coefficients indicated in Figure 10B (yellow surface) show areas where a favorable interaction between a substituent and the probe determines a decrease in activity, whereas an unfavorable interaction between a substituent and the probe determines an increase in activity; in this picture, three main regions (A', G', H') and six other secondary regions (B'–F', I') were recognized.

Table 1. AT1 Antagonists Used for the 3D-QSAR Study

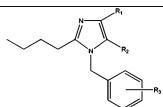
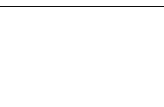
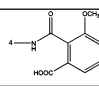
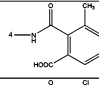
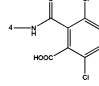
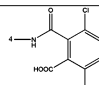
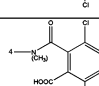
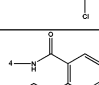
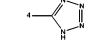
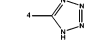
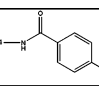
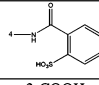
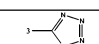
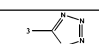
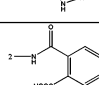
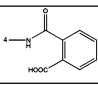
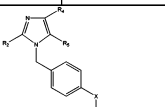
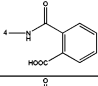
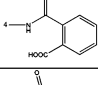
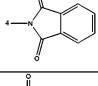
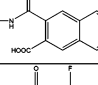
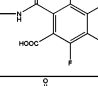
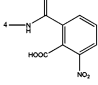
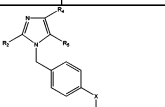
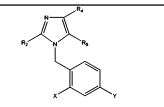
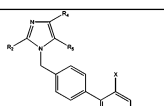
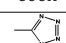
																		
Compd	R ₁	R ₂	R ₃	IC ₅₀ (μM)	Compd	R ₁	R ₂	R ₃	IC ₅₀ (μM)									
1 ⁴¹	Cl	CH ₂ COOH	4-COOH	1.6	22 ⁴¹	Cl	CH ₂ COOCH ₃		0.08									
2 ⁴¹	Cl	CH ₂ COOCH ₃	4-NH ₂	100	23 ⁴¹	Cl	CH ₂ COOCH ₃		0.032									
3 ⁴¹	CH ₂ COOH	Cl	4-COOH	19	24 ⁴¹	Cl	CH ₂ COOCH ₃		0.018									
4 ⁴¹	Cl	CH ₂ OH	4-COOH	1.7	25 ⁴¹	Cl	CH ₂ OCH ₃		0.042									
5 ⁴¹	CH ₂ OH	Cl	4-COOH	100	26 ⁴¹	Cl	CH ₂ OCH ₃		5.70									
6 ⁴¹	Cl	CH ₂ OAc	4-COOH	5.3	27 ⁴¹	Cl	CH ₂ COOCH ₃		0.19									
7 ⁴¹	Cl	CH ₂ COOH	4-CH ₂ COOH	13	28 ⁴¹	Cl	CH ₂ COOCH ₃	4-NHCOF ₃	27									
8 ⁴¹	Cl	CH ₂ COOCH ₃	4-NO ₂	100	29 ⁴¹	Cl			1.2									
9 ⁴¹	Cl	CH ₂ COOCH ₃	4-NHCH ₂ Ph	40	30 ⁴¹	Cl	CH ₂ COOCH ₃		11									
10 ⁴¹	Cl	CH ₂ OH	4-CHO	28	31 ⁴¹	Cl	CH ₂ OCH ₃		0.012									
11 ⁴¹	Cl	CH ₂ OH	4-OCH ₃	100	32 ⁴¹	Cl	CH ₂ COOH	3-COOH	100									
12 ⁴¹	Cl	CH ₂ COOCH ₃	4-NHCO(CH ₂) ₂ COOH	46	33 ⁴¹	Cl	CH ₂ COOH	2-COOH	38									
13 ⁴¹	Cl	CH ₂ COOCH ₃	4-NHCO(CH ₂) ₂ COOH	32	34 ⁴¹	Cl			3.8									
14 ⁴¹	Cl	CH ₂ COOCH ₃	4-NHCOCH=CHCOOH (cis)	11	35 ⁴¹	Cl	CH ₂ COOCH ₃		100									
15 ⁴¹	Cl	CH ₂ COOCH ₃		0.14														
16 ⁴¹	CH ₂ COOCH ₃	Cl		0.42														
17 ⁴¹	Cl	CH ₂ OCH ₃		0.28														
18 ⁴¹	Cl	CH ₂ COOCH ₃		3.1														
19 ⁴¹	Cl	CH ₂ COOCH ₃		5.8														
20 ⁴¹	Cl	CH ₂ COOCH ₃		0.79														
21 ⁴¹	Cl	CH ₂ COOCH ₃		0.40														
																		
Compd	R ₂	R ₄	R ₅	X						A	IC ₅₀ (μM)	Compd	R ₂	R ₄	R ₅	X	Y	IC ₅₀ (μM)
54 ⁴³	<i>n</i> -C ₄ H ₉	Cl	CH ₂ COOH	Cl						H	40	55 ⁴³	<i>n</i> -C ₄ H ₉	Cl	CH ₂ COOH	NO ₂	H	13
																		
Compd	R ₂	R ₄	R ₅	X	IC ₅₀ (μM)													
56 ⁴³	<i>n</i> -C ₄ H ₉	Cl	CH ₂ OH	COOH	0.3													
57 ⁴³	<i>n</i> -C ₄ H ₉	Cl	COOH	COOH	0.092													
58 ⁴³	<i>n</i> -C ₄ H ₉	Cl	CHO	COOH	0.94													
59 ⁴³	<i>n</i> -C ₄ H ₉	H	CHO	COOH	0.55													
60 ⁴³	C ₂ H ₅ CH=CH	Cl	CH ₂ OH	COOH	0.08													
61 ⁴³	C ₂ H ₅ CH=CH	Cl	CHO	COOH	0.33													
62 ⁴³	<i>n</i> -C ₄ H ₉	Cl	CH ₂ OH		0.019													
36 ⁴²	<i>n</i> -C ₄ H ₉	Cl	CH ₂ OH	none	3-COOH	0.49												
37 ⁴²	<i>n</i> -C ₄ H ₉	H	CH ₂ OH	none	3-COOH	1.1												
38 ⁴²	<i>n</i> -C ₄ H ₉	Cl	CH ₂ OCOCH ₃	none	3-COOH	2.5												
39 ⁴²	<i>n</i> -C ₄ H ₉	Cl	CH ₂ OCH ₃	none	3-COOH	2.9												
40 ⁴²	<i>n</i> -C ₄ H ₉	Cl	CH ₂ OH	CO	2-COOH	0.16												
41 ⁴²	<i>n</i> -C ₄ H ₉	CH ₂ OH	Cl	CO	2-COOH	0.34												
42 ⁴²	<i>n</i> -C ₄ H ₉	CH ₂ OCOCH ₃	Cl	CO	2-COOH	1.4												
43 ⁴²	<i>n</i> -C ₄ H ₉	Cl	CH ₂ NHCO ₂ CH ₃	CO	2-COOH	0.27												
44 ⁴²	<i>n</i> -C ₄ H ₉	Cl	CH ₂ OCH ₃	CO	2-COOH	0.15												
45 ⁴²	<i>n</i> -C ₄ H ₉	Cl	CH ₂ OH	O	2-COOH	0.40												
46 ⁴²	<i>n</i> -C ₄ H ₉	Cl	CH ₂ OH	S	2-COOH	0.40												
47 ⁴²	<i>n</i> -C ₄ H ₉	Cl	CH ₂ OH	OCH ₂	2-COOH	0.92												
48 ⁴²	<i>n</i> -C ₄ H ₉	H	CH ₂ OH	OCH ₂	2-COOH	0.31												
49 ⁴²	<i>n</i> -C ₄ H ₉	Cl	CH ₂ OCOCH ₃	OCH ₂	2-COOH	1.8												
50 ⁴²	<i>n</i> -C ₄ H ₉	Cl	CH ₂ OCH ₃	OCH ₂	2-COOH	1.2												
51 ⁴²	<i>n</i> -C ₄ H ₉ S	H	CH ₂ OH	OCH ₂	2-COOH	5.9												
52 ⁴²	<i>n</i> -C ₄ H ₉ S	H	CH ₂ OH	OCH ₂	2-COOH	12												
53 ⁴²	<i>n</i> -C ₄ H ₉	Cl	CH ₂ OH	Trans-CH=CH	2-COOH	5.4												

Table 2. Statistical Results of the 3D-QSAR Models Obtained with the Training Set ($n = 52$) and the Test Set ($n = 10$)

model	grid probes	vars	PC	r^2	q^2	SDEP _{cv}	SDEP _{test-set}
1	C3	1168	5	0.98	0.72	0.57	0.64
2	OH	1086	4	0.97	0.76	0.52	0.54
3	C3 and OH	2011	5	0.98	0.74	0.54	0.60

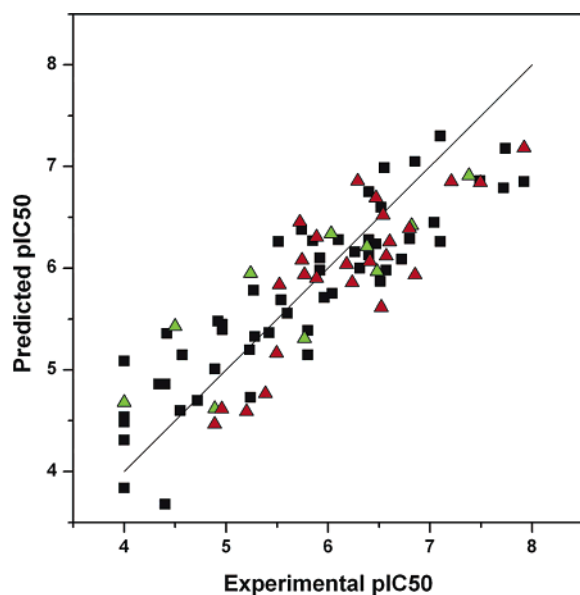
**Figure 9.** Plot of model 2. Experimental vs predicted pIC_{50} is reported. The first test set is represented with green triangles, while the second test set is represented with red triangles.

Figure 10C–F illustrates compounds **31**, **40**, **47**, and **7** embedded in their activity plot contributions; a positive contribution to the activity is colored green, while a negative contribution to the activity is colored red.

Figure 10C shows that the sulfonate group of **31** (characterized by the best IC_{50} value, $0.012 \mu M$) interacts favorably with the regions C, D, and E, while the unsubstituted nitrogen of the imidazole group interacts with region A. As regards the yellow regions that give a positive contribution to the activity plot, they might be considered as hydrophobic contributions that increase the activity of the ligand; in the case of **31**, the *n*-butyl chain interacts favorably with region A', the sulfonate phenyl ring with H' and G', and the chlorine atom with region C'.

Compound **40** is approximately 13-fold less potent than **31** and is characterized by the presence of a 2-benzoylbenzoate substituent instead of the biphenyl-2-sulfonate, and the hydroxymethyl substituent instead of the methoxymethyl. Figure 10D shows that the carboxylate function interacts favorably with regions E and D, while the hydroxymethyl group interacts with region B and the carboxylic function interacts favorably with region F. However, with respect to **31**, the presence of the 2-benzoylbenzoate group determines the shift of the ligand, with the loss of interaction with regions C and A. As regards the steric contributions, the interactions with A', C', G', and H' are maintained.

The presence of the 2-(phenoxy)methylbenzoate instead of the 2-benzoylbenzoate determines a decrease in activity: compound **47** differs from **40** only in the presence of the oxymethylene group, and it is about six times less active. As shown in Figure 10E, the absence of the carboxylic function determines the loss of the favorable interaction with region F and a reduction in the interaction of the carboxylic group with the region E.

Compound **7** displays a low activity ($IC_{50} = 13 \mu M$), seeing that the substitution of the benzoate group with an acetate

Table 3. Structure and Binding Data of the Ligands Used as Second Test Set

Compd	R ₁	R ₂	R ₃	R ₄	IC ₅₀ (μM)
63st	CH ₂ OCH ₃	<i>n</i> -C ₄ H ₉	Cl	2-CONHOH	4.1
64st	CH ₂ OH	<i>n</i> -C ₄ H ₉	Cl	2-CONHSO ₂ Ph	0.14
65st	CH ₂ OH	<i>n</i> -C ₄ H ₉	Cl	2-NHCOCF ₃	6.3
66st	CH ₂ OCH ₃	<i>n</i> -C ₄ H ₉	Cl		0.032
67st	CHO	<i>n</i> -C ₄ H ₉	Cl		13
68st	CH ₂ OCH ₃	<i>n</i> -C ₄ H ₉	Cl		0.30
69st	CH ₂ OH	<i>n</i> -C ₄ H ₉	Cl	4-COOH	11.0
70st	CH ₂ OH	<i>n</i> -C ₄ H ₉	Cl	3-CH ₃ -2-COOH	1.9
71st	CH ₂ OH	<i>n</i> -C ₄ H ₉	Cl	6-OCH ₃ -2-COOH	3.0
72st	CH ₂ OH	<i>n</i> -C ₄ H ₉	Cl	4-OCH ₃ -2-CN ₂ H	0.58
73st	CH ₂ OH	<i>n</i> -C ₄ H ₉	Cl	5-CN-2-CN ₂ H	0.51
74st	CH ₂ OH	C ₆ H ₅	Cl	2-COOH	1.70
75st	CH ₂ OH	<i>n</i> -C ₄ H ₉	Cl	2-COOH	0.16
76st	CH ₂ OH	<i>n</i> -C ₄ H ₉	Cl	2-COOH	1.30
77st	CH ₂ OH	<i>n</i> -C ₄ H ₉	H	2-COOH	0.27
78st	CH ₂ OH	<i>n</i> -C ₄ H ₉	CF ₃	2-COOH	0.062
79st	CH ₂ OH	<i>n</i> -C ₄ H ₉	CH ₃	2-COOH	1.8
80st	CH ₂ OH	<i>n</i> -C ₄ H ₉	CF ₃		0.012
81st	CH ₂ NH ₂	<i>n</i> -C ₄ H ₉	Cl	2-COOH	3.2
82st	CH ₂ NHCOOCH ₃	<i>n</i> -C ₄ H ₉	Cl	2-COOH	0.25
83st	CH ₂ NHCOOCH ₂ CH=CH ₂	<i>n</i> -C ₄ H ₉	Cl	2-COOH	0.39
84st		<i>n</i> -C ₄ H ₉	Cl		0.29
85st	CH=NNHSO ₂ Ph	<i>n</i> -C ₄ H ₉	Cl		0.66
86st	COOCH ₃	<i>n</i> -C ₄ H ₉	Cl	2-COOH	0.34
87st	CON(CH ₃) ₂	<i>n</i> -C ₄ H ₉	Cl	2-COOH	1.3
Model 1 Model 2 Model 3					
SDEP _{Test-Set}	0.52	0.49	0.50		

determines the loss of interaction with regions E, D, and G', as shown in Figure 10F.

Because the alignment of the ligands was performed using the structures docked into the AT1 receptor, it was likely to be useful to check for matching between the AT1 receptor and the 3D-QSAR maps.

In Figure 11, the binding site of the AT1 receptor overlaps with the 3D PLS coefficient maps. There is a close match between the receptor and the PLS surfaces: region A is in proximity of Y113, region B corresponds to Q6.52(257), while

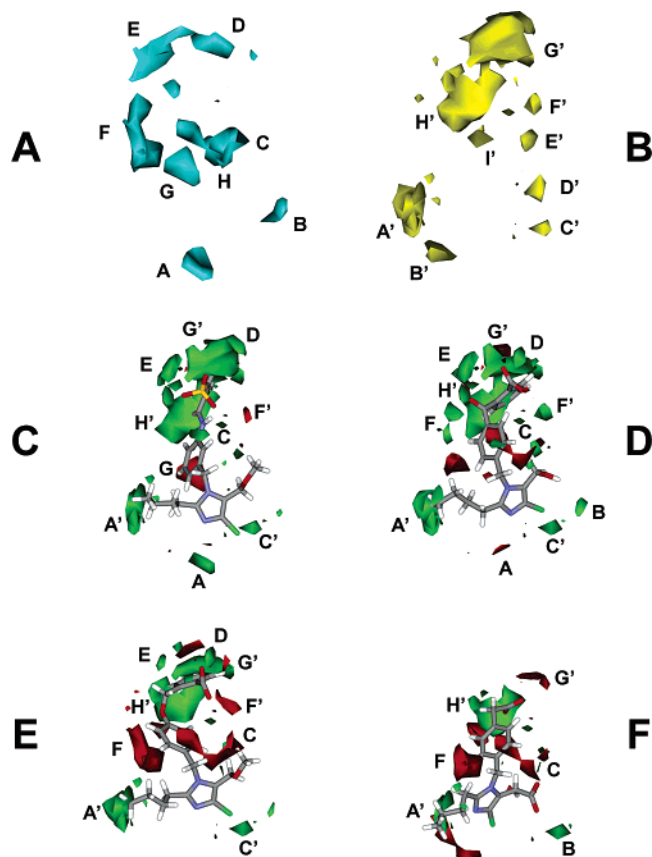


Figure 10. Negative (A) and positive (B) regions of the PLS coefficient plot obtained with the OH probe. The activity contributions plots (green polyhedrons represent positive contributions, whereas red polyhedrons represent negative contributions to the activity) for compounds **31** (C), **40** (D), **47** (E), and **7** (F) were also reported.

C comprises K5.42(199) and Y184. Region D corresponds to T175, region E is between the backbone of C180 and S3.29(105), and F is between S3.29(105) and S3.33(109). As regards the yellow surfaces, regions A' and B' correspond to the secondary lipophilic pocket principally created by Y3.37(113), A4.60(163), and F171, and region E' corresponds to H6.51(256). Finally, of the main regions G' and H', the former is very close to V179 and I7.39(288), while region H' corresponds to V3.32(108).

Conclusions

We have constructed a 3D model of the AngII receptor AT₁, based on crystallized bovine rhodopsin.¹¹

The docking of losartan into the AT₁ receptor confirmed that K5.42(199), V3.32(108), and A4.60(163) interacted with the ligand, in agreement with mutagenesis data.^{15,16} As regards the anionic tetrazole ring of losartan, it did not appear to interact with any residue suggested as important by mutagenesis data, and in particular, in contrast with the recent published AT₁ homology models,^{17,21} it did not interact with K5.42(199). Otherwise it was principally stabilized by a H bond with Y184 and further interactions with T175 and H6.51(256).

Residues D2.50(74), N3.35(111), S3.39(115), N7.45(294), and N7.46(295) interacted with each other, forming a H bond network system able to connect TM2, TM3, and TM7: because site-direct mutagenesis suggested their fundamental role in the activation process of the receptor,^{18,28–31} they probably control the inactive–active state of the receptor. This speculation is in agreement with the last structurally related activation mechanisms proposed for the AT₁ receptor.²⁶ It hypothesized, during the activation, the breaking of the main interactions between

TM2, TM3, and TM7 and the following rotation of TM3 accompanied by the exclusion of TM7 from the water-filled crevice forming the binding pocket of the AT₁ receptor.

As regards the insurmountable interaction of EXP3174, it was explained by a strong binding interaction; moreover, the model was in agreement with the important role of the interaction of K5.42(199) and Q6.52(257) with the insurmountable antagonists EXP3174, candesartan, valsartan, and irbesartan.^{17,32}

Finally, a 3D-QSAR model was developed using the alignment obtained through an automated docking procedure for 62 non-peptide antagonists and the good correlation obtained supported the reliability of the constructed AT₁ receptor model.

In conclusion, this study illustrates a new hypothesis about the binding interaction of non-peptide antagonists inside the AT₁ receptor, encouraging further investigations on new residues that might be fundamental for the ligand–receptor interaction. Furthermore, because AT₁ antagonists are an interesting therapeutic target, the information obtained, combined with the calculated 3D-QSAR model, may allow a predictive affinity evaluation of newly designed non-peptide antagonists.

Experimental Section

Amino Acid Numbering. To refer to specific amino acid sequences, the numbering system suggested by Ballesteros and Weinstein is used.⁴⁶

The most highly conserved residue in each transmembrane helix (TMH) is assigned a value of 0.50, and this number is preceded by the TMH number and followed in parentheses by the sequence number. The other residues in the helix are given a locant value relative to this.

Homology Modeling. The crystal structure of bovine rhodopsin was taken from the Protein Data Bank,⁴⁷ while all the primary sequences were obtained from the SWISS–PROT protein sequence database.⁴⁸

The sequential alignment of bovine rhodopsin and the AT receptors was performed by means of CLUSTAL W,⁴⁹ using the Blosom series as a matrix, with a gap open penalty of 10 and a gap extension penalty of 0.05.

The TM helices and the first and second intracellular and extracellular loops of the AT₁ receptor were constructed directly from the coordinates of the corresponding amino acids in rhodopsin by means of the Modeller program.¹³ Because the amino acid length differs from the template, the other loop regions were constructed by means of the “Loop optimization method” of Modeller, applying the “very_slow” loop refinement method. During the construction of the receptor and the loop refinement, the presence of a disulfide bridge between C101 and C180 was taken into account, because it was present in bovine rhodopsin; furthermore, as suggested by mutagenesis studies,⁵⁰ we considered also the formation of a disulfide bridge between C18 and C274.

Starting from this receptor, 10 structures were generated by means of the “very slow MD annealing” refinement method, as implemented in Modeller, and on the basis of the DOPE (discrete optimized protein energy) assess method, the best receptor model was chosen. The backbone conformation of the resulting receptor structure was evaluated by inspection of the ψ/ϕ Ramachandran plot obtained from PROCHECK analysis.¹⁴

Docking of Losartan and EXP3174. The ligands were submitted to a conformational search of 1000 steps with an energy window for saving structure of 10 kJ/mol by means of the MACROMODEL program.⁵¹ The algorithm used was the Monte Carlo method with MMFFs as the force field and a distance-dependent dielectric constant of 1.0. The ligands were then minimized using the conjugated gradient method until a convergence value of 0.05 kcal/(Å·mol), using the same force field and dielectric constant used for the conformational search. Both ligands were docked into the AT₁ receptor using the AUTODOCK 3.0 program.²⁰ The regions of interest used by AUTODOCK were defined by considering atom

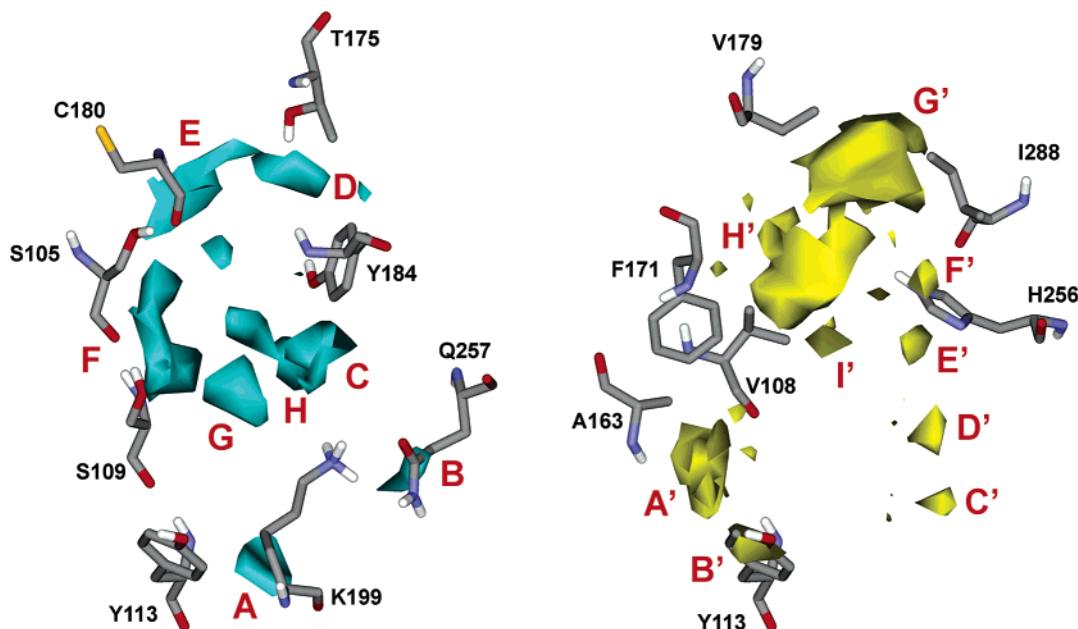


Figure 11. PLS coefficient plots obtained with the OH probe superimposed to the AT1 receptor binding site.

CZ3 of W6.48(253) as the central residue of a grid of 50, 44, and 48 points in the x , y , and z directions with the result that the main residues suggested as important by site-directed mutagenesis were considered. A grid spacing of 0.375 Å and a distance-dependent function of the dielectric constant were used for the energy map calculations.

Using the Lamarckian genetic algorithm, we subjected the compound to 100 runs of the AUTODOCK search, in which the default values of the other parameters were used. Cluster analysis was performed on the docked results using an RMS tolerance of 1.0 Å.

The best two docking conformations were complexed with the AT1 receptor and then subjected to MD simulations.

MD Simulations. All simulations were performed using AMBER 8.⁵² The two complexes were embedded into a previously stabilized phospholipid bilayer made up of DPPC molecules. The receptor–ligand complexes were manually inserted into the entry of the DPPC bilayer in such a way that the α helices of the receptor were oriented approximately parallel to the hydrocarbon chains of the phospholipids. After that, all phospholipids within a radius of 1 Å around the receptor were deleted.

MD simulations were carried out using the modified parm94 force field at 300 K. An explicit solvent model TIP3P water was used, and the system was solvated on the “extracellular” and “intracellular” side with a 15 Å water cap. Chlorine ions were added as counterions to neutralize the system. Prior to MD simulations, three steps of minimization were carried out; in the first stage, we kept the protein and phospholipids fixed with a constraint of 500 kcal/mol, and we just minimized the positions of the water molecules; then in the second stage, we minimized the phospholipids–water system applying a constraint of 500 kcal/mol on the protein, and finally in the last step, we applied a constraint of 50 kcal/mol only on the α carbons of the receptor. The three minimization stages consisted of 5000 steps in which the first 1000 were steepest descent (SD) and the last 4000 conjugate gradient (CG). Molecular dynamics trajectories were run using the minimized structure as a starting input, and the particle mesh Ewald (PME) algorithm was used for dealing with long-range interactions.⁵³ The time step of the simulations was 2.0 fs with a cutoff of 12 Å for the nonbonded interaction, and SHAKE was employed to keep all bonds involving hydrogen atoms rigid. Constant-volume was carried out for 100 ps, during which the temperature was raised from 0 to 300 K (using the Langevin dynamics method); then 900 ps of constant-pressure MD was carried out at 300 K. In the first 400 ps of MD, all the α carbons of the receptor were blocked with

a harmonic force constant, which decreased during these 400 ps from 50 to 1 kcal/(mol·Å), while in the last 600 ps, there were no constraints. The final structure of the complexes was obtained as the average of the last 500 ps of MD minimized with the CG method until a convergence of 0.05 kcal/(Å·mol).

General Amber force field (GAFF) parameters were assigned to ligands and DPPC molecules, while the partial charges were calculated using the AM1-BCC method as implemented in the Antechamber suite of AMBER 8.

The phospholipid bilayer system was previously stabilized by 600 ps of MD using the same parameters described above. Prior to MD simulations, two steps of minimization were carried out; in the first stage, we kept the phospholipids fixed with a constraint of 500 kcal/mol, and we just minimized the positions of the water molecules; then in the second stage, we minimized the phospholipids–water system applying a constraint of 100 kcal/mol on the heavy atom of the phospholipids. In the first 200 ps of MD, all the heavy atoms of the DPPC molecules were blocked with a harmonic force constant, which decreased during these 200 ps from 100 to 10 kcal/(mol·Å), while in the last 400 ps, there were no constraints. The structure of the bilayer system in which the two AT1 receptor complexes were embedded was obtained as the average of the last 300 ps of MD minimized with the CG method until a convergence of 0.05 kcal/(Å·mol).

Docking of Insurmountable Antagonists. Candesartan, irbersartan, and valsartan were docked into the AT1 receptor using the minimized average of the last 500 ps of MD simulations of the AT1–EXP3174 complex as the receptor. The regions of interest used by AUTODOCK were defined by considering EXP3174 complexed into AT1 as the central group; in particular, a grid of 40, 40, and 48 points in the x , y , and z directions was constructed, centered on the center of the mass of this antagonist. A grid spacing of 0.375 Å and a distance-dependent function of the dielectric constant were used for the energy map calculations.

Using the Lamarckian genetic algorithm, we subjected the docked compounds to 100 runs of the AUTODOCK search, in which the default values of the other parameters were used. Cluster analysis was performed on the results, using an RMS tolerance of 1.0 Å, and the best docked structures were considered (which for irbersartan and valsartan corresponded also to the most populated cluster).

3D-QSAR. Alignment of the Molecules. The ligands shown in Table 1 were docked into the AT1 receptor, using the same procedure seen above for the insurmountable antagonists, but the

minimized average of the last 500 ps of MD simulations of the AT1–losartan complex were used as the receptor.

All the carboxylate, sulfonate, and tetrazole ring substituents were treated as fully ionized groups. For each ligand, the best docked structure was chosen, and this receptor-based alignment was used for further studies. For most of the ligands, the first cluster corresponded also to the most populated one.

None of the ligands reported in the literature that showed more than six AUTODOCK atom types were taken into consideration, due to the limits of the software.

Before construction of the 3D-QSAR model, the binding free energy calculated for each ligand–AT1 complex by means of the AUTODOCK scoring function was correlated with the experimental antagonist affinity, but the quadratic correlation (R^2) showed a low value ($R^2 < 0.4$).

Data Set. The GOLPE program⁴⁵ was used to define three 3D-QSAR models, using GRID interaction fields⁵⁴ as descriptors (see below). The training set was composed of 52 compounds, characterized by affinity values spanning about 4 orders of magnitude, the minimum value of 4.00 (expressed as $-\log IC_{50}$) being associated with compounds **2**, **5**, **8**, **32**, and **35** and the maximum value of 7.92 being associated with compound **31**. Similarly, compounds belonging to the test set showed an affinity value ranging from 4.0 (compound **11**) to 7.38 (compound **25**) and were uniformly distributed along the activity range (see Figure 9).

Probe Selection. The GRID program⁵⁴ was used to describe the previously superimposed molecular structure. Interaction energies between selected probes and each molecule were calculated using a grid spacing of 1 Å. C3 (corresponding to a methyl group), OH (corresponding to a phenolic OH group) and a combination of them were used to calculate the molecular interaction fields (MIFs). Beyond these two probes, in this study were also used: O (sp^2 carbonyl oxygen), OH2 (water), C1= (sp^2 CH aromatic or vinyl), and DRY (hydrophobic) probes, and the best results (q^2 , SDEP_{Cv}, and SDEP_{test-set}) were obtained with the OH and C3 probes.

Variable Selection. The MIFs of the training set were imported into GOLPE; it is well-known that many of the variables deriving from GRID analysis could be considered as noise, which decreases the quality of the model. For this reason, variable selection was operated by zeroing values with absolute values smaller than 0.06 kcal/mol and removing variables with a standard deviation below 0.1. Moreover, variables that exhibited only two values and had a skewed distribution were also removed.

The smart region definition (SRD) algorithm⁵⁵ was applied with 10% of the active variables as the number of seed (selected in the PLS weights space), a critical distance cutoff of 2.5 Å, and a collapsing distance cutoff of 4.0 Å. The groups were then used in the fractional factorial design (FFD) procedure. FFD selection was applied twice, until the r^2 and q^2 values did not increase significantly, using the cross-validation routine with five random sets of compounds.

Acknowledgment. Many thanks are due to Prof. Gabriele Cruciani and Prof. Sergio Clementi (Molecular Discovery and MIA srl) for the use of the GOLPE program in their chemometric laboratory (University of Perugia, Italy) and for having provided the GRID program.

References

- Juillerat-Jeanneret, L.; Celerier, J.; Chapuis Bernasconi, C.; Nguyen, G.; Wostl, W.; Maerki, H. P.; Janzer, R. C.; Corvol, P.; Gasc, J. M. Renin and angiotensinogen expression and functions in growth and apoptosis of human glioblastoma. *Br. J. Cancer* **2004**, *90*, 1059–1068.
- Fogarty, D. J.; Sanchez-Gomez, M. V.; Matute, C. Multiple angiotensin receptor subtypes in normal and tumor astrocytes in vitro. *Glia* **2002**, *39*, 304–313.
- Henrion, D.; Kubis, N.; Levy, B. I. Physiological and pathophysiological functions of the AT(2) subtype receptor of angiotensin II: from large arteries to the microcirculation. *Hypertension* **2001**, *38*, 1150–1157.
- Weber, M. A. Angiotensin II receptor blockers and cardiovascular outcomes: what does the future hold? *JRAAS* **2003**, *4*, 62–73.
- Manohar, P.; Pina, I. L. Therapeutic role of angiotensin II receptor blockers in the treatment of heart failure. *Mayo Clin. Proc.* **2003**, *78*, 334–338.
- Norris, K.; Vaughn, C. The role of renin-angiotensin-aldosterone system inhibition in chronic kidney disease. *Exp. Rev. Cardiovasc. Ther.* **2003**, *1*, 51–63.
- Mimran, A.; Ribstein, J. Angiotensin receptor blockers: pharmacology and clinical significance. *J. Am. Soc. Nephrol.* **1999**, *S12*, S273–S277.
- Panek, R. L.; Lu, G. H.; Overhiser, R. W.; Major, T. C.; Hodges, J. C.; Taylor, D. G. Functional studies but not receptor binding can distinguish surmountable from insurmountable AT1 antagonism. *J. Pharmacol. Exp. Ther.* **1995**, *273*, 753–761.
- Timmermans, P. B. Pharmacological properties of angiotensin II receptor antagonists. *Can. J. Cardiol.* **1999**, *15* (Suppl F), 26F–28F.
- De Gasparo, M.; Catt, K. J.; Inagami, T.; Wright, J. W.; Unger, T. International union of pharmacology. XXIII. The angiotensin II receptors. *Pharmacol. Rev.* **2000**, *52*, 415–472.
- Okada, T.; Sugihara, M.; Bondar, A. N.; Elstner, M.; Entel, P.; Buss, V. The retinal conformation and its environment in rhodopsin in light of a new 2.2 Å crystal structure. *J. Mol. Biol.* **2004**, *342*, 571–583.
- Baldwin, J. M.; Schertler, G. F.; Unger, V. M. An alpha-carbon template for the transmembrane helices in the rhodopsin family of G-protein-coupled receptors. *J. Mol. Biol.* **1997**, *272*, 144–164.
- Fiser, A.; Do, R. K.; Sali, A. Modeling of loops in protein structures. *Protein Sci.* **2000**, *9*, 1753–1773.
- Laskowski, R. A.; MacArthur, M. W.; Moss, D. S.; Thornton, J. M. PROCHECK: a program to check the stereochemical quality of protein structures. *J. Appl. Crystallogr.* **1993**, *26*, 283–291.
- Noda, K.; Saad, Y.; Kinoshita, A.; Boyle, T. P.; Graham, R. M.; Husain, A.; Karnik, S. S. Tetrazole and carboxylate groups of angiotensin receptor antagonists bind to the same subsite by different mechanisms. *J. Biol. Chem.* **1995**, *270*, 2284–2289.
- Ji, H.; Leung, M.; Zhang, Y.; Catt, K. J.; Sandberg, K. Differential structural requirements for specific binding of nonpeptide and peptide antagonists to the AT1 angiotensin receptor. Identification of amino acid residues that determine binding of the antihypertensive drug losartan. *J. Biol. Chem.* **1994**, *269*, 16533–16536.
- Takezako, T.; Gogonea, C.; Saad, Y.; Noda, K.; Karnik, S. S. “Network leaning” as a mechanism of insurmountable antagonism of the angiotensin II type 1 receptor by non-peptide antagonists. *J. Biol. Chem.* **2004**, *279*, 15248–15257.
- Balmforth, A. J.; Lee, A. J.; Warburton, P.; Donnelly, D.; Ball, S. G. The conformational change responsible for AT1 receptor activation is dependent upon two juxtaposed asparagine residues on transmembrane helices III and VII. *J. Biol. Chem.* **1997**, *272*, 4245–4251.
- Hines, J.; Fluharty, S. J.; Yee, D. K. Structural determinants for the activation mechanism of the angiotensin II type 1 receptor differ for phosphoinositide hydrolysis and mitogen-activated protein kinase pathways. *Biochem. Pharmacol.* **2003**, *66*, 251–262.
- Morris, G. M.; Goodsell, D. S.; Halliday, R. S.; Huey, R.; Hart, W. E.; Belew, R. K.; Olson, A. J. Automated docking using a Lamarckian genetic algorithm and empirical binding free energy function. *J. Comput. Chem.* **1998**, *19*, 1639–1662.
- Zoumpoulakis, P.; Daliani, I.; Zervou, M.; Kyrikou, I.; Siapi, E.; Lamprinidis, G.; Mikros, E.; Mavromoustakos, T. Losartan’s molecular basis of interaction with membranes and AT1 receptor. *Chem. Phys. Lipids* **2003**, *125*, 13–25.
- Mehler, E. L.; Periole, X.; Hassan, S. A.; Weinstein, H. Key issues in the computational simulation of GPCR function: representation of loop domains. *J. Comput.-Aided Mol. Des.* **2002**, *16*, 841–853.
- Mavromoustakos, T.; Daliani, I.; Matsoukas, J. The application for biophysical methods to study drug: membrane interactions. In *Bioactive Peptides in Drug Discovery and Design: Medical Aspects*; Matsoukas, J., Mavromoustakos, T., Eds.; Biomedical and Health Research, Vol. 22; IOS Press-Ohmsha: Amsterdam, 1999; pp 13–24.
- Theodoropoulou, E.; Marsh, D. Interactions of angiotensin II non-peptide AT(1) antagonist losartan with phospholipid membranes studied by combined use of differential scanning calorimetry and electron spin resonance spectroscopy. *Biochim. Biophys. Acta* **1999**, *1461*, 135–146.
- Boucard, A. A.; Roy, M.; Beaulieu, M. E.; Lavigne, P.; Escher, E.; Guillemette, G.; Leduc, R. Constitutive activation of the angiotensin II type 1 receptor alters the spatial proximity of transmembrane 7 to the ligand-binding pocket. *J. Biol. Chem.* **2003**, *278*, 36628–36636.
- Martin, S. S.; Boucard, A. A.; Clement, M.; Escher, E.; Leduc, R.; Guillemette, G. Analysis of the third transmembrane domain of the human type 1 angiotensin II receptor by cysteine scanning mutagenesis. *J. Biol. Chem.* **2004**, *279*, 51415–51423.

- (27) Clement, M.; Martin, S. S.; Beaulieu, M. E.; Chamberland, C.; Lavigne, P.; Leduc, R.; Guillemette, G.; Escher, E. Determining the environment of the ligand binding pocket of the human angiotensin II type I (hAT1) receptor using the methionine proximity assay. *J. Biol. Chem.* **2005**, *280*, 27121–27129.
- (28) Doan, T. N.; Ali, M. S.; Bernstein, K. E. Tyrosine kinase activation by the angiotensin II receptor in the absence of calcium signaling. *J. Biol. Chem.* **2001**, *276*, 20954–20958.
- (29) Le, M. T.; Vanderheyden, P. M.; Szaszak, M.; Hunyady, L.; Kersemans, V.; Vauquelin, G. Peptide and nonpeptide antagonist interaction with constitutively active human AT1 receptors. *Biochem. Pharmacol.* **2003**, *65*, 1329–1338.
- (30) Hunyady, L.; Ji, H.; Jagadeesh, G.; Zhang, M.; Gaborik, Z.; Mihalik, B.; Catt, K. J. Dependence of AT1 angiotensin receptor function on adjacent asparagine residues in the seventh transmembrane helix. *Mol. Pharmacol.* **1998**, *54*, 427–434.
- (31) Monnot, C.; Bihoreau, C.; Conchon, S.; Curnow, K. M.; Corvol, P.; Clauser, E. Polar residues in the transmembrane domains of the type 1 angiotensin II receptor are required for binding and coupling. Reconstitution of the binding site by coexpression of two deficient mutants. *J. Biol. Chem.* **1996**, *271*, 1507–1513.
- (32) Fierens, F. L.; Vanderheyden, P. M.; Gaborik, Z.; Minh, T. L.; Backer, J. P.; Hunyady, L.; Ijzerman, A.; Vauquelin, G. Lys(199) mutation of the human angiotensin type 1 receptor differentially affects the binding of surmountable and insurmountable non-peptide antagonists. *JRAAS* **2000**, *3*, 283–288.
- (33) Pandya, T.; Pandey, S. K.; Tiwari, M.; Chaturvedi, S. C.; Saxena, A. K. 3-D-QSAR studies of triazolinone based balanced AT1/AT2 receptor antagonists. *Bioorg. Med. Chem.* **2001**, *9*, 291–300.
- (34) Kurup, A.; Gary, R.; Carini, D. J.; Hansch, C. Comparative QSAR: Angiotensin II antagonists. *Chem. Rev.* **2001**, *101*, 2727–2750.
- (35) Krovat, E. M.; Langer, T. Non-peptide angiotensin II receptor antagonists: chemical feature based pharmacophore identification. *J. Med. Chem.* **2003**, *46*, 716–726.
- (36) Datar, P. A.; Desai, P. V.; Coutinho, E. C. A 3D-QSAR of angiotensin II (AT1) receptor antagonists based on receptor surface analysis. *J. Chem. Inf. Comput. Sci.* **2004**, *44*, 210–220.
- (37) Cappelli, A.; Pericot Mohr, G. G.; Gallelli, A.; Rizzo, M.; Anzini, M.; Vomero, S.; Mennuni, L.; Ferrari, F.; Makovec, F.; Menziani, M. C.; De Benedetti, P. G.; Giorgi, G. Design, synthesis, structural studies, biological evaluation, and computational simulations of novel potent AT(1) angiotensin II receptor antagonists based on the 4-phenylquinoline structure. *J. Med. Chem.* **2004**, *47*, 2574–2586.
- (38) Yoo, S. E.; Kim, S. K.; Lee, S. H.; Yi, K. Y.; Lee, D. W. A comparative molecular field analysis and molecular modelling studies on pyridylimidazole type of angiotensin II antagonists. *Bioorg. Med. Chem.* **1999**, *7*, 2971–2976.
- (39) Belvisi, L.; Bravi, G.; Catalano, G.; Mabilia, M.; Salimbeni, A.; Scolastico, C. A 3D QSAR CoMFA study of non-peptide angiotensin II receptor antagonists. *J. Comput.-Aided Mol. Des.* **1996**, *10*, 567–582.
- (40) Datar, P.; Desai, P.; Coutinho, E.; Iyer, K. CoMFA and CoMSIA studies of angiotensin (AT1) receptor antagonists. *J. Mol. Model.* **2002**, *8*, 290–301.
- (41) Duncia, J. V.; Chiu, A. T.; Carini, D. J.; Gregory, G. B.; Johnson, A. L.; Price, W. A.; Wells, G. J.; Wong, P. C.; Calabrese, J. C.; Timmermans, P. B. The discovery of potent nonpeptide angiotensin II receptor antagonists: a new class of potent antihypertensives. *J. Med. Chem.* **1990**, *33*, 1312–1329.
- (42) Carini, D. J.; Duncia, J. V.; Johnson, A. L.; Chiu, A. T.; Price, W. A.; Wong, P. C.; Timmermans, P. B. Nonpeptide angiotensin II receptor antagonists: N-[(benzyloxy)benzyl]imidazoles and related compounds as potent antihypertensives. *J. Med. Chem.* **1990**, *33*, 1330–1336.
- (43) Wong, P. C.; Price, W. A., Jr; Chiu, A. T.; Carini, D. J.; Duncia, J. V.; Johnson, A. L.; Wexler, R. R.; Timmermans, P. B. Nonpeptide angiotensin II receptor antagonists. Studies with EXP9270 and DuP 753. *Hypertension* **1990**, *15*, 823–834.
- (44) Carini, D. J.; Duncia, J. V.; Aldrich, P. E.; Chiu, A. T.; Johnson, A. L.; Pierce, M. E.; Price, W. A.; Santella, J. B., 3rd; Wells, G. J.; Wexler, R. R.; et al. Nonpeptide angiotensin II receptor antagonists: the discovery of a series of N-(biphenylmethyl)imidazoles as potent, orally active antihypertensives. *J. Med. Chem.* **1991**, *34*, 2525–2547.
- (45) *GOLPE 4.5*. Multivariate Infometric Analysis Srl., Viale dei Castagni 16, Perugia, Italy, 1999.
- (46) Ballesteros, J. A.; Weinstein, H. W. Integrated methods for the construction of three-dimensional models and computational probing of structure–function relations in G-protein coupled receptors. *Methods Neurosci.* **1995**, *25*, 366–428.
- (47) Berman, H. M.; Westbrook, J.; Feng, Z.; Gilliland, G.; Bhat, T. N.; Weissig, H.; Shindyalov, I. N.; Bourne, P. E. The Protein Data Bank. *Nucleic Acids Res.* **2000**, *28*, 235–242.
- (48) Gasteiger, E.; Gattiker, A.; Hoogland, C.; Ivanyi, I.; Appel, R. D.; Bairoch, A. ExPASy: the proteomics server for in-depth protein knowledge and analysis. *Nucleic Acids Res.* **2003**, *31*, 3784–3788.
- (49) Thompson, J. D.; Higgins, D. G.; Gibson, T. J. CLUSTAL W: improving the sensitivity of progressive multiple sequence alignment through sequence weighting, position-specific gap penalties and weight matrix choice. *Nucleic Acids Res.* **1994**, *22*, 4673–4680.
- (50) Heering, J. N.; Hines, J.; Fluharty, S. J.; Yee, D. K. Identification and function of disulfide bridges in the extracellular domains of the angiotensin II type 2 receptor. *Biochemistry* **2001**, *40*, 8369–8377.
- (51) *Macromodel*, ver. 8.5; Schrödinger Inc.: Portland, OR, 1999.
- (52) Case, D. A.; Darden, T. A.; Cheatham, T. E., III; Simmerling, C. L.; Wang, J.; Duke, R. E.; Luo, R.; Merz, K. M.; Wang, B.; Pearlman, D. A.; Crowley, M.; Brozell, S.; Tsui, V.; Gohlke, H.; Mongan, J.; Hornak, V.; Cui, G.; Beroza, P.; Schafmeister, C.; Caldwell, J. W.; Ross, W. S.; Kollman, P. A. *AMBER 8*; University of California, San Francisco: 2004.
- (53) Darden, T.; Darrin, Y.; Pedersen, L. Particle mesh Ewald: An N·log(N) method for Ewald sums in large systems. *J. Chem. Phys.* **1993**, *98*, 10089–10092.
- (54) Cruciani, G.; Goodford, P. Copyright Molecular Discovery Ltd. 2001–2003 GREATER graphical interface for GRID version, 1.1.7 GRIB, UPF/IMIM, Barcelona (Spain) <http://www.moldiscovery.com>.
- (55) Pastor, M.; Cruciani, G.; Clementi, S. Smart region definition: a new way to improve the predictive ability and interpretability of three-dimensional quantitative structure–activity relationships. *J. Med. Chem.* **1997**, *40*, 1455–1464.

JM060338P